COMPUTER METHODS AND PROGRAMS IN BIOMEDICINE XXX (2013) XXX–XXX

journal homepage: www.intl.elsevierhealth.com/journals/cmpb

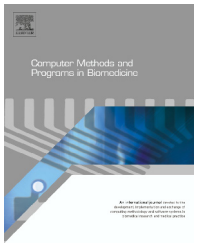

Kinematics based sensory fusion for wearable motion assessment in human walking

S. Šlajpah, R. Kamnik, M. Munih*

University of Ljubljana, Faculty of Electrical Engineering, Tržaška cesta 25, 1000 Ljubljana, Slovenia

ARTICLE INFO

Article history:
Received 29 July 2013
Received in revised form
25 October 2013
Accepted 20 November 2013

Keywords:
Sensory fusion
Kinematic model
Extended Kalman filter
Inertial measurement unit
Measuring insoles
Long-term walking

ABSTRACT

Measuring the kinematic parameters in unconstrained human motion is becoming crucial for providing feedback information in wearable robotics and sports monitoring. This paper presents a novel sensory fusion algorithm for assessing the orientations of human body segments in long-term human walking based on signals from wearable sensors. The basic idea of the proposed algorithm is to constantly fuse the measured segment's angular velocity and linear acceleration via known kinematic relations between segments. The wearable sensory system incorporates seven inertial measurement units attached to the human body segments and two instrumented shoe insoles. The proposed system was experimentally validated in a long-term walking on a treadmill and on a polygon with stairs simulating different activities in everyday life. The outputs were compared to the reference parameters measured by a stationary optical system. Results show accurate joint angle measurements (error median below 5°) in all evaluated walking conditions with no expressed drift over time.

1. Introduction

Wearable robotics and monitoring in sports are two recently developed fields where the latest progress in sensory technology contributed essentially. Introduction of micro-electromechanical systems (MEMS) components enabled production of miniature, low power, and inexpensive sensors. MEMS components are convenient to be worn by the user [1] or to be implemented on a wearable robotic structure, such as active prostheses [2,3], orthoses [4,5], and exoskeletons [6,7]. Wearable sensory system is ought to provide information on kinematic (e.g. joint angles) and kinetic (e.g. feet reactions) parameters. The acquired information is used for providing the feedback to the user [8–10] or for closing the loop in a robot controller [4,11–13].

Level-ground human walking is considered a basic manoeuver of human locomotion and as such has been subject of numerous studies in recent decades [14,15]. The algorithms for on-line processing of the sensory signals have been evolving together with growth of computational power on microcontrollers and knowledge about mechanisms of walking. In the first attempts, the uni-axial gyroscopes attached to body segments were used to assess joint angles with a simple integration method [16–19]. The method is prone to the output drift over long-term measurements since it integrates superimposed noise over time. To overcome the problem of drift a solution was proposed as a system reset and re-initialization of the outputs with regards to a known reference value at each gait cycle [16]. In [17,18] authors introduced additional accelerometers to determine the mid stance phase in each stride and to estimate an inclination of the segment.

* *Corresponding author*. Tel.: +386 1 4768 355.
E-mail addresses: sebastjan.slajpah@fe.uni-lj.si (S. Šlajpah), roman.kamnik@fe.uni-lj.si (R. Kamnik), marko.munih@fe.uni-lj.si (M. Munih).
0169-2607/$ – see front matter © 2013 Elsevier Ireland Ltd. All rights reserved.
http://dx.doi.org/10.1016/j.cmpb.2013.11.012

Nomenclature

$\boldsymbol{a}_A$	linear acceleration of point A
$\boldsymbol{a}_B$	linear acceleration of point B
$\boldsymbol{\omega}$	angular velocity
$\boldsymbol{r}_{AB}$	position vector connection A to B
${}^{I}\boldsymbol{\omega}$	angular velocity measured by IMU
${}^{I}\boldsymbol{a}$	linear acceleration measured by IMU
${}^{I}\mathbf{B}$	magnetic field measured by IMU
${}^{E}\boldsymbol{a}_1$	linear acceleration of the previous joint
${}^{E}\boldsymbol{a}_2$	linear acceleration of the following joint
${}^{S}\boldsymbol{r}_1$	vector between previous joint and IMU
${}^{S}\boldsymbol{r}_2$	vector between IMU and following joint
${}^{S}\boldsymbol{g}$	gravity vector
${}^{S}\boldsymbol{q}_I$	quaternion describing IMU's orientation in segment's coordinate frame
${}^{S}\boldsymbol{a}_{DYN}$	dynamic acceleration
${}^{E}\boldsymbol{q}$	quaternion describing the segment's orientation
${}^{E}\mathbf{B}$	Earth's magnetic field
${}^{E}\boldsymbol{q}(0)$	quaternion describing initial segment's orientation
${}^{S}\mathbf{B}(0)$	initial magnetic field
${}^{E}\mathbf{R}(0)$	rotation matrix describing initial segment's orientation in Earth's frame
${}^{S}\boldsymbol{a}(0)$	initial linear acceleration
$\boldsymbol{f}$	function relating two sequential state vectors
$\boldsymbol{h}_k$	function relating the state to the measurement
$\boldsymbol{x}_k$	state vector
$\boldsymbol{z}_k$	measurement vector
$\boldsymbol{u}_{k-1}$	input vector
$\boldsymbol{w}_{k-1}$	process noise
$\boldsymbol{v}_k$	measurement noise
${}^{E}\dot{\boldsymbol{q}}$	first time derivative of quaternion ${}^{E}\boldsymbol{q}$
${}^{E}\ddot{\boldsymbol{q}}$	second time derivative of quaternion ${}^{E}\boldsymbol{q}$
Δt	time difference
$\mathbf{P}_k^-$	error covariance
$\mathbf{A}_k$	Jacobian matrix of the $\boldsymbol{f}$ with respect to $\boldsymbol{x}$
$\mathbf{Q}_k$	process noise covariance matrix
$\mathbf{W}_k$	process Jacobian matrix
$\mathbf{K}_k$	EKF gain matrix
$\mathbf{H}_k$	Jacobian matrix of the $\boldsymbol{h}$ with respect to $\boldsymbol{x}$
$\mathbf{R}_k$	measurement noise covariance matrix
$\mathbf{V}_k$	measurement Jacobian matrix
${}^{S}h_1$	height of the IMU placement on the foot
${}^{S}\mathrm{COP}_{X,1}$	COP in the X direction
${}^{S}\mathrm{COP}_{Z,1}$	COP in the Z direction

The inclination estimate was then used to reset the integration of angular velocity. Mayagoitia et al. [19] used accelerometers under static conditions to assess the reference angle needed for the calculation of segmental orientation. Difficulty with this approach is that during fast uninterrupted walking it is impossible to accomplish accurate re-initialization. Besides, this approach is not suitable for real-time applications due to computationally demanding algorithms.

The problem of the integrational drift can be also avoided by using only accelerometers for joint angle assessment. Presented methods [20,21] do not implement the integration of angular velocity but are built upon comparison of accelerations at the center point of rotation obtained from sensors placed on two adjacent segments. Willemsen et al. [20] calculated joint angles using data from pairs of two uniaxial accelerometers in two dimensions. Authors stressed that angle error increases with increasing the speed of motion. Dejnadabi et al. [21] presented a methodology of utilizing a combination of accelerometer and gyroscope per segment. The approach estimates the acceleration of the joint center by virtually placing a pair of sensors at the rotation center. Authors split the motion of the individual segment into linear and angular motion and thus utilize relation between acceleration and angular velocity. Joint angle is determined by comparing the acceleration of the rotational point expressed in adjacent segments and considering the rotation between the segments. The accuracy of the algorithm is conditioned with the anatomical aspect of the individual subject. In [22] authors introduced an array of accelerometers mounted on a rigid rod. The angle of individual segment is determined by band pass filtering of the difference between measured accelerations from two sensors. Experimental validation of the algorithms was accomplished only at low speeds of walking (below 2 km/h) with obtained accuracy below 6°. Similar approach was presented by Liu et al. [23] as double-sensor difference based method utilizing two accelerometers per segment for orientation estimate. The difference between two sensors mounted on the same segment is expressed only with the rotational acceleration while the gravitational and linear accelerations, skin motion artifact, and other noise are eliminated when measured acceleration data are mutually subtracted.

Luinge and Veltink [24] introduced the use of Kalman filter for assessing the orientation of individual segment by fusing data from gyroscope and accelerometer. The orientation estimate obtained by integration of the 3D angular velocity is continuously corrected by using inclination estimate obtained from measured acceleration of the segment. The results show that due to the heading drift the presented method is not suitable for long-term measurements. Also the performance of Kalman filter is significantly reduced when estimating the orientation of fast moving segment [25]. Similar, Favre et al. [26] presented quaternion-based fusion of gyroscope and accelerometer data. The correction of the integrated segment's orientation was performed by estimating inclination angle via accelerometer when the segment was not undergoing fast motion. Presented method is accurate only for a short time motion assessment. In [27] authors used angular velocity to differ between translational and gravitational component in measured acceleration. The orientation of the segment is determined by assessing the inclination from resultant acceleration. Authors stated that gait at higher velocities influence the accuracy considerable and that sensor placement must be taken into consideration.

Common to the methods above is that they operate with respect to one reference axis which is gravity. With this technique only segment's orientation in two dimensions can be determined. To measure three-dimensional orientation,

Please cite this article in press as: S. Šlajpah, et al., Kinematics based sensory fusion for wearable motion assessment in human walking, Comput. Methods Programs Biomed. (2013), http://dx.doi.org/10.1016/j.cmpb.2013.11.012

additional reference axis needs to be introduced. Veltink et al. [28] used the direction of motion progression as the second reference axis to successfully monitor the foot 3D orientation during gait. More common, magnetometers have been incorporated into the systems using magnetic field as the additional axis [29–32]. Algorithm presented by O'Donovan et al. [29] is based on dividing movements to static and dynamic. During dynamic movement the orientation estimate is obtained by integrating data from gyroscope while during quasi-static movement the orientation is described regarding gravity and magnetic field. The performance of the technique was validated only for short-term quasi-static moves. In [32] authors implemented the Unscented Kalman filter for orientation estimation. Estimate obtained by integrating angular velocity is corrected in every sample by the orientation estimated via accelerometer and magnetometer. During fast movement this method yields larger errors in orientation since it is not differentiating between gravitational and dynamical components of measured acceleration. Roetenberg et al. [30] presented complementary Kalman filter which is based on estimating errors between orientation obtained by integrating gyroscope data and one obtained from accelerometer and magnetometer. Additional model of magnetometer was introduced to improve the performance of the orientation estimation algorithms in the vicinity of the ferromagnetic materials. In [31] additional magnetic tracking system has been implemented for the same reason. Commercially available XSens MVN motion capture suit (XSens, Enschede, The Netherlands) [33] is assessing the pose of the individual body segments by implementing prediction and correction step. During prediction, inertial navigation system predicts the segment's pose which is then extended to prediction based on kinematics relations. During correction step, updates based on biomechanical characteristic of the human body, detection of contacts, and additional aiding sensors (e.g. GPS, barometers, cameras) are performed.

The experimental validation of the presented approaches from the literature was limited by the number of steps that can be accomplished in the field of view of the reference system (e.g. Optotrak, Vicon) and lasted only up to 30 s. In the literature, to the best knowledge of authors, no experiments were found for testing the wearable sensors in long-term and dynamic walking conditions.

The aim of this paper is to present a novel approach for long-term kinematic parameters assessment with a combined use of inertial, magnetic, and insole sensors. The approach is based on fusing measured accelerations and angular velocities with calculated accelerations based on human body kinematic relations. In the following chapters we present the extended Kalman filter algorithm with incorporated kinematic model for orientation estimation of a single body segment. The approach is further extended to seven segments of human body lower extremities with recursive procedure and switching mechanism based on foot loading information. The accuracy and long-term reliability of proposed approach are experimentally evaluated by comparison to reference measurement system in treadmill walking at different speeds and walking on a polygon with stairs.

2. Methods

2.1. Wearable sensors

Wearable sensory system comprises seven inertial and magnetic measurement units (IMUs) placed on segments of lower extremities and trunk. Besides, two instrumented measuring shoe insoles are used for measuring feet reaction forces.

An IMU consists of three digital sensors: a three-axis gyroscope (measuring range ±500°/s), a three-axis accelerometer (measuring range ±4 G) and a three-axis magnetometer (measuring range ±1.3 Ga) [32]. The size of one unit is (30 × 20 × 5) mm and weight of 6 g. Each IMU is equipped with an onboard 8-bit processor and a 2.4 GHz wireless transmission system. Measured data from individual IMU are wirelessly transferred to a data acquisition unit with a 100 Hz refresh rate.

Parotec-System pressure measurement shoe insoles (Paromed GmbH, Neubeuern, Germany) consist of 24 hydrocell sensors each [34] and measure reaction forces of different anatomical points of foot and load distribution along the feet. A vertical reaction force of the feet and position of the center of pressure (COP) under each foot can be extracted from measured data. A custom on-board processing unit is used for data acquisition and real-time transfer. Each insole sensor was previously calibrated for proper pressure-to-force conversion. The insole acquisition system is operating with sampling frequency of 100 Hz.

2.2. Kinematic relation in serial kinematic chain

The sensory fusion for estimating segment's orientations in long-term and dynamic motion proposed in this paper is built upon an extended Kalman filter (EKF) algorithm [35,36]. The concept is based on a kinematic relation (1) which states that on a rigid body the acceleration of any point can be determined if the angular velocity, angular acceleration and linear acceleration of other point on the body are known

$$\boldsymbol{a}_B = \boldsymbol{a}_A + \boldsymbol{\omega} \times (\boldsymbol{\omega} \times \boldsymbol{r}_{AB}) + \dot{\boldsymbol{\omega}} \times \boldsymbol{r}_{AB} \quad (1)$$

where $\boldsymbol{a}_A$ and $\boldsymbol{a}_B$ state for linear acceleration of points A and point B on a body, respectively. $\boldsymbol{\omega}$ is angular velocity, $\dot{\boldsymbol{\omega}}$ is time derivative of angular velocity representing angular acceleration, and $\boldsymbol{r}_{AB}$ is position vector between A and B. Eq. (1) is in proposed algorithm used to relate the linear acceleration of location where the IMU is attached to the segment (point B) and linear acceleration of segment's joint center (point A).

A serial kinematic chain of rigid bodies mimicking human lower extremities, of which on each segment one IMU is placed, is presented in Fig. 1. Quantities marked with subscript j are referring to a corresponding j-th segment. Vectors ${}^{I}\boldsymbol{\omega}$, ${}^{I}\boldsymbol{a}$ and ${}^{I}\mathbf{B}$ represent vectors of angular velocity, linear acceleration and magnetic field measured by IMU sensor, respectively. Measured values are expressed in IMU's coordinate frame what is denoted with left superscript I. Vector ${}^{E}\boldsymbol{a}_1$ is denoting the linear acceleration of the center point of the joint connecting j-th segment with the previous $j-1$ segment. Vector ${}^{E}\boldsymbol{a}_2$ denotes the linear acceleration of the center point

Please cite this article in press as: S. Šlajpah, et al., Kinematics based sensory fusion for wearable motion assessment in human walking, Comput. Methods Programs Biomed. (2013), http://dx.doi.org/10.1016/j.cmpb.2013.11.012

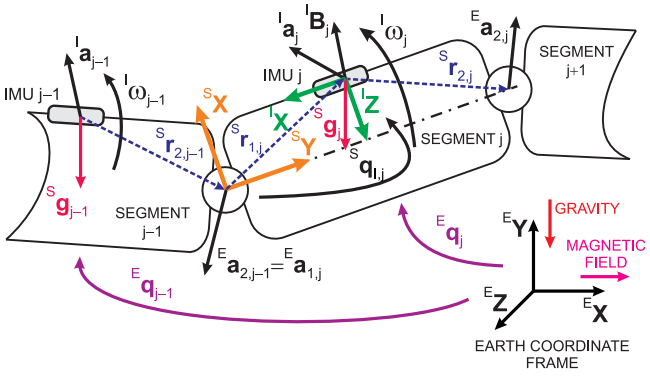

Fig. 1 – A serial kinematic chain of segments with marked connections between two neighboring segments and IMU's measured quantities. Quantities marked with subscripts *j* and *j* – 1 are referring to *j*-th and (*j* – 1)-th segment, respectively. Quantities marked left with superscripts I, S, and E are expressed in the coordinate frame of the IMU, segment, and Earth, respectively.

of the joint connecting the *j*-th segment with the following *j*+1 segment. Left superscripts E indicates that the quantity is expressed in the Earth's coordinate frame which is formed by the gravity vector (^{E}Y axis) and a normal vector to a plane described with gravity and magnetic vectors (^{E}Z axis). Vector pointing from joint which connects segments $j-1$ and j to the IMU and vectors pointing from IMU to joint which connects segments j and $j+1$ are denoted as $^{S}\boldsymbol{r}_1$ and $^{S}\boldsymbol{r}_2$. Left superscripts S denotes that quantities are expressed in the segment's coordinate system. The vectors describe the geometric model of the segment and also determine how the IMU is placed on the segment. Gravity vector is marked with $^{S}\boldsymbol{g}$. Quaternion $^{E}\boldsymbol{q}$ is describing the segment's orientation with respect to the Earth coordinate frame. A quaternion notation is used to avoid singularities which are common in other representations of orientations such as Euler angles or homogenous matrices.

By substituting variables depicted in Fig. 1 in (1), the relation between measured acceleration from the IMU $^{S}\boldsymbol{a}$ and the linear acceleration of the center point of joint connecting segment *j* with the previous one $^{S}\boldsymbol{a}_1$ can be described as

$$^{S}\boldsymbol{a}_j = {}^{S}\boldsymbol{a}_{1,j} + {}^{S}\boldsymbol{\omega}_j \times ({}^{S}\boldsymbol{\omega}_j \times {}^{S}\boldsymbol{r}_{1,j}) + {}^{S}\dot{\boldsymbol{\omega}}_j \times {}^{S}\boldsymbol{r}_{1,j} - {}^{S}\boldsymbol{g}_j. \tag{2}$$

Since the IMU is not positioned on the segment in a way that its axes would be aligned with the axes of the segment's local coordinate system, the measured quantities are transformed into the segment's coordinate system by Eqs. (3)–(5). The relation between the segment's and IMU's coordinate frames is described with quaternion $^{S}\boldsymbol{q}_I$

$$[0, {}^{S}\boldsymbol{\omega}]^{T} = {}^{S}\boldsymbol{q}_I \otimes [0, {}^{I}\boldsymbol{\omega}]^{T} \otimes {}^{S}\boldsymbol{q}_I^{*} \tag{3}$$

$$[0, {}^{S}\boldsymbol{a}]^{T} = {}^{S}\boldsymbol{q}_I \otimes [0, {}^{I}\boldsymbol{a}]^{T} \otimes {}^{S}\boldsymbol{q}_I^{*} \tag{4}$$

$$[0, {}^{S}\boldsymbol{B}]^{T} = {}^{S}\boldsymbol{q}_I \otimes [0, {}^{I}\boldsymbol{B}]^{T} \otimes {}^{S}\boldsymbol{q}_I^{*} \tag{5}$$

where $\otimes$ represents a quaternion multiplication and * denotes a conjugated quaternion. In Eq. (2) the measured linear acceleration $^{S}\boldsymbol{a}$ is composed of dynamic $^{S}\boldsymbol{a}_{DYN}$ and gravitational $^{S}\boldsymbol{g}$ contributions:

$$^{S}\boldsymbol{a}_I = {}^{S}\boldsymbol{a}_{DYN} - {}^{S}\boldsymbol{g}. \tag{6}$$

Gravity vector is transformed into segment's local coordinate frame as

$$[0, {}^{S}\boldsymbol{g}]^{T} = {}^{E}\boldsymbol{q}^{*} \otimes [0, {}^{E}\boldsymbol{g}]^{T} \otimes {}^{E}\boldsymbol{q} \tag{7}$$

where $^{E}\boldsymbol{g} = [0, -9.81, 0]^{T}$ m/s^2.

Similarly as in (2), Eq. (1) is also used to express the relationship between measured linear acceleration $^{S}\boldsymbol{a}$ and linear acceleration of the center point of the joint connecting segment *j* with the following one $^{S}\boldsymbol{a}_2$

$$^{S}\boldsymbol{a}_{2,j} = {}^{S}\boldsymbol{a}_j + {}^{S}\boldsymbol{\omega}_j \times ({}^{S}\boldsymbol{\omega}_j \times {}^{S}\boldsymbol{r}_{2,j}) + {}^{S}\dot{\boldsymbol{\omega}}_j \times {}^{S}\boldsymbol{r}_{2,j} + {}^{S}\boldsymbol{g}_j. \tag{8}$$

If the acceleration at the connection point with the previous segment $^{S}\boldsymbol{a}_{2,j-1}$ is known, and if it is transformed into the Earth's coordinate frame

$$[0, {}^{E}\boldsymbol{a}_{2,j-1}]^{T} = {}^{E}\boldsymbol{q}_{j-1} \otimes [0, {}^{S}\boldsymbol{a}_{2,j-1}]^{T} \otimes {}^{E}\boldsymbol{q}_{j-1}{}^{*} \tag{9}$$

the result can also be used as linear acceleration $^{S}\boldsymbol{a}_{1,j}$ of the *j*-th segment

$$^{E}\boldsymbol{a}_{1,j} = {}^{E}\boldsymbol{a}_{2,j-1} \tag{10}$$

which expressed in the coordinate frame of the *j*-th segment

$$[0, {}^{S}\boldsymbol{a}_{1,j}]^{T} = {}^{E}\boldsymbol{q}_j{}^{*} \otimes [0, {}^{E}\boldsymbol{a}_{1,j}]^{T} \otimes {}^{E}\boldsymbol{q}_j \tag{11}$$

is used in (2). Set of Eqs. (2), (9), (11), and (8) form a basis for iterative procedure processing a serial kinematic chain of lower extremities segments.

Vector of the magnetic field $^{I}\boldsymbol{B}$, measured by the IMU and expressed in the segment's frame, as shown in (5), is modeled as rotated magnetic field of the Earth in the Earth's coordinate frame $^{E}\boldsymbol{B}$. Due to declination and inclination of the Earth's magnetic field, the initial vector of the global magnetic field is observed as

$$[0, {}^{E}\boldsymbol{B}]^{T} = {}^{E}\boldsymbol{q}(0) \otimes [0, {}^{S}\boldsymbol{B}(0)]^{T} \otimes {}^{E}\boldsymbol{q}(0)^{*} \tag{12}$$

where $^{E}\boldsymbol{q}(0)$ denotes the initial quaternion describing the rotation from the Earth's coordinate frame to the segment initial measurement. This initial rotation is determined by a rotational matrix $^{E}\mathbf{R}(0)$

$$^{E}\mathbf{R}(0) = [\boldsymbol{x}|\boldsymbol{y}|\boldsymbol{z}] = \begin{cases} \boldsymbol{x} \rightarrow \boldsymbol{y} \times \boldsymbol{z} \\ \boldsymbol{y} \rightarrow {}^{S}\boldsymbol{a}(0) \\ \boldsymbol{z} \rightarrow {}^{S}\boldsymbol{B}(0) \times {}^{S}\boldsymbol{a}(0) \end{cases}. \tag{13}$$

$^{S}\boldsymbol{a}(0)$ and $^{S}\boldsymbol{B}(0)$ in (13) are initial linear acceleration and magnetic field, respectively. Initial measurement must be accomplished in a standstill, thus assessing only gravitational

Please cite this article in press as: S. Šlajpah, et al., Kinematics based sensory fusion for wearable motion assessment in human walking, Comput. Methods Programs Biomed. (2013), http://dx.doi.org/10.1016/j.cmpb.2013.11.012

vector (see (6)). Similarly to the gravity (see (7)), the measured magnetic vector can be described as

$$[0, {}^{S}\mathbf{B}]^{T} = {}^{E}\mathbf{q}^{*} \otimes [0, {}^{E}\mathbf{B}]^{T} \otimes {}^{E}\mathbf{q}. \tag{14}$$

2.3. *Model-based extended Kalman filter*

An extended Kalman filter (EKF) algorithm [36] is used to fuse the measured data from IMU sensors and knowledge about the lengths of the segments and sensor placement. The estimation model combines angular velocity integration with relations (2) and (14). The model incorporates a non-linear state-space presentation of state and measurement equations

$$\begin{aligned} \mathbf{x}_k &= f(\mathbf{x}_{k-1}, \mathbf{u}_{k-1}, \mathbf{w}_{k-1}) \\ \mathbf{z}_k &= h(\mathbf{x}_k, \mathbf{v}_k). \end{aligned} \tag{15}$$

The non-linear function f describes the relations between the state vector $\mathbf{x}_k$ at time step k and the state $\mathbf{x}_{k-1}$, the input vector $\mathbf{u}_{k-1}$ and superimposed process noise $\mathbf{w}_{k-1}$ at time step $k-1$. The function $\mathbf{h}_k$ relates the state to the measurements $\mathbf{z}_k$ at time step k with addition of superimposed measurement noise $\mathbf{v}_k$.

The state vector $\mathbf{x}_k$ in proposed algorithm for single segment orientation assessment is defined as

$$\mathbf{x}_k = [{}^{S}\boldsymbol{\omega} \quad {}^{S}\dot{\boldsymbol{\omega}} \quad {}^{E}\mathbf{q} \quad {}^{E}\dot{\mathbf{q}} \quad {}^{E}\ddot{\mathbf{q}}]^{T} \tag{16}$$

with ${}^{E}\dot{\mathbf{q}}$ and ${}^{E}\ddot{\mathbf{q}}$ being the first and the second time derivative of quaternion ${}^{E}\mathbf{q}$. The function f of the state equation is given as follows: $f_{[1-3]}$ represents time integration of angular velocity ${}^{S}\boldsymbol{\omega}$ and $f_{[4-6]}$ forward transfer of angular acceleration. The time integration of quaternion ${}^{E}\mathbf{q}$ is described with $f_{[7-10]}$, while $f_{[11-14]}$ and $f_{[15-18]}$ represent the first and the second time derivative of the quaternion ${}^{E}\mathbf{q}$ as stated in [37]. Combined function f is presented with Eq. (17)

$$\begin{bmatrix} f_{[1-3]} \\ f_{[4-6]} \\ f_{[7-10]} \\ f_{[11-14]} \\ f_{[15-18]} \end{bmatrix} = \begin{bmatrix} {}^{S}\boldsymbol{\omega} + {}^{S}\dot{\boldsymbol{\omega}}_{I}\Delta t \\ {}^{S}\dot{\boldsymbol{\omega}} \\ {}^{E}\mathbf{q} + {}^{E}\dot{\mathbf{q}}\Delta t \\ \frac{1}{2}{}^{E}\mathbf{q} \otimes [0, \quad {}^{S}\boldsymbol{\omega}]^{T} \\ \frac{1}{2}{}^{E}\dot{\mathbf{q}} \otimes [0, \quad {}^{S}\boldsymbol{\omega}]^{T} + \frac{1}{2}{}^{E}\mathbf{q} \otimes [0, \quad {}^{S}\dot{\boldsymbol{\omega}}]^{T} \end{bmatrix} \tag{17}$$

where Δt represents the time difference between two sequential time steps.

The measurement vector incorporates all measured quantities and is defined as

$$\mathbf{z}_k = [{}^{S}\boldsymbol{\omega} \quad {}^{S}\dot{\boldsymbol{\omega}} \quad {}^{S}\boldsymbol{a} \quad {}^{S}\mathbf{B}]^{T}. \tag{18}$$

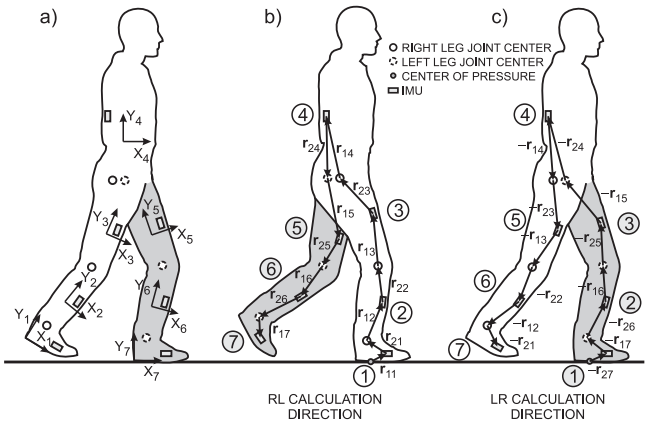

Fig. 2 – (a) Presentation of orientations of coordinate systems of individual segments. Origins of segmental coordinate systems are set in the joint centers; (b) right–left (RL) sequence of orientation calculations, denoted with numbers in circles, when the right foot is in stance phase (vectors r are expressed in corresponding segment coordinate frame); (c) left–right (LR) sequence of orientation calculations when the left foot is in stance phase. Left superscripts S are omitted to increase the clarity of the figure.

The function $\mathbf{h}$ relates measured quantities with state space variables through (2) and (14). The function $\mathbf{h}$ is given as

$$\begin{bmatrix} \mathbf{h}_{[1-3]} \\ \mathbf{h}_{[4-6]} \\ \mathbf{h}_{[7-9]} \\ [0, \mathbf{h}_{[10-12]}]^{T} \end{bmatrix} = \begin{bmatrix} {}^{S}\boldsymbol{\omega} \\ {}^{S}\dot{\boldsymbol{\omega}} \\ {}^{S}\boldsymbol{a}_1 + {}^{S}\boldsymbol{\omega} \times ({}^{S}\boldsymbol{\omega} \times {}^{S}\mathbf{r}_1) + {}^{S}\dot{\boldsymbol{\omega}} \times {}^{S}\mathbf{r}_1 - {}^{S}\boldsymbol{g} \\ {}^{E}\mathbf{q}^{*} \otimes [0, {}^{E}\mathbf{B}]^{T} \otimes {}^{E}\mathbf{q} \end{bmatrix}. \tag{19}$$

The set of equations for discrete-time EKF algorithm implementation is adopted from [36]. The time update projects the current state estimate ahead in time. The time update equations are combined with ahead projection of the state $\hat{\mathbf{x}}_k^-$ (20) and the error covariance $\mathbf{P}_k^-$ (21)

$$\hat{\mathbf{x}}_k^- = f(\hat{\mathbf{x}}_{k-1}, \mathbf{u}_{k-1}, 0) \tag{20}$$

$$\mathbf{P}_k^- = \mathbf{A}_k\mathbf{P}_{k-1}\mathbf{A}_k^{T} + \mathbf{W}_k\mathbf{Q}_{k-1}\mathbf{W}_k^{T}. \tag{21}$$

The measurement update adjusts the projected estimate by an actual measurement at that time. The filter gain matrix $\mathbf{K}_k$ (22) is calculated and used to update the state and covariance estimates based on the measurement innovation as shown in (23) and (24)

$$\mathbf{K}_k = \mathbf{P}_k^-\mathbf{H}_k^{T}(\mathbf{H}_k\mathbf{P}_k^-\mathbf{H}_k^{T} + \mathbf{V}_k\mathbf{R}_k\mathbf{V}_k^{T})^{-1} \tag{22}$$

$$\hat{\mathbf{x}}_k = \hat{\mathbf{x}}_k^- + \mathbf{K}_k(\mathbf{z}_k - h(\hat{\mathbf{x}}_k^-, 0)) \tag{23}$$

$$\mathbf{P}_k = (I - \mathbf{K}_k\mathbf{H}_k)\mathbf{P}_k^-. \tag{24}$$

Please cite this article in press as: S. Šlajpah, et al., Kinematics based sensory fusion for wearable motion assessment in human walking, Comput. Methods Programs Biomed. (2013), http://dx.doi.org/10.1016/j.cmpb.2013.11.012

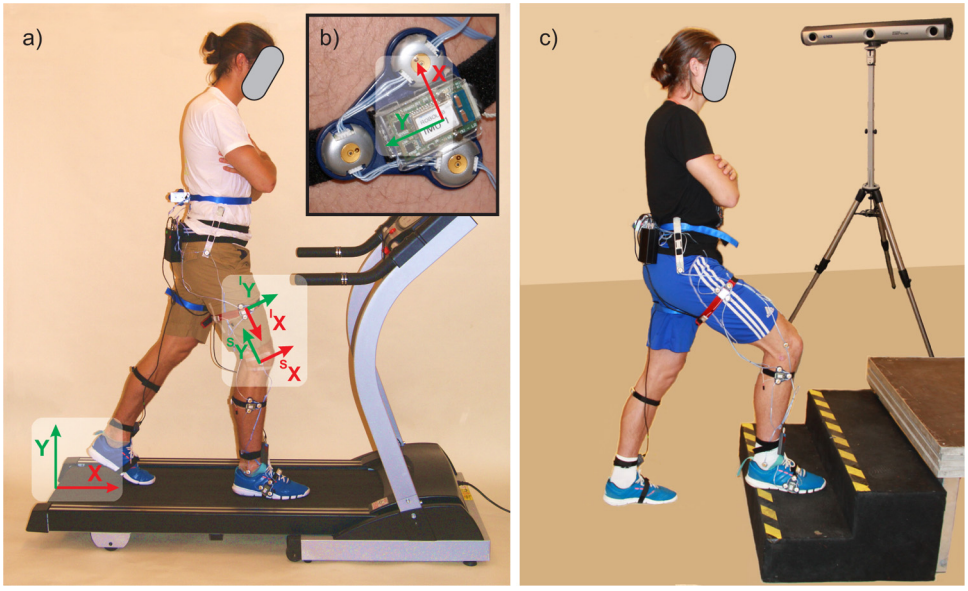

Fig. 3 – (a) Experimental test setup: subject with IMUs, measuring shoe insoles, and Optotrak markers walking on a treadmill; (b) IMU on a measuring plate with corresponding infrared markers; (c) subject equipped with sensors walking up the stairs on the polygon.

Matrices $\mathbf{A}_k$ and $\mathbf{H}_k$ are calculated by linearizing equations (15) around $\hat{\mathbf{x}}_k^-$ at each time step k. Matrix $\mathbf{A}_k$ relates the states at the previous time step $k-1$ to the state at the current step k and is computed as

$$\mathbf{A}_k^{[i,j]} = \frac{\partial f^{[i]}}{\partial x^{[j]}}(\hat{\mathbf{x}}_{k-1}, \mathbf{u}_{k-1}, 0). \tag{25}$$

Matrix $\mathbf{H}_k$ relates the state to the measurement $\mathbf{z}_k$ and is determined as

$$\mathbf{H}_k^{[i,j]} = \frac{\partial h^{[i]}}{\partial x^{[j]}}(\hat{\mathbf{x}}_k, 0). \tag{26}$$

Matrices $\mathbf{Q}_k$ and $\mathbf{R}_k$ are the process noise covariance matrix and the measurement noise covariance matrix, respectively. The process Jacobians $\mathbf{W}_k$ and the measurement Jacobians $\mathbf{V}_k$ are assumed to be constant and thus presented as identity matrices. The EKF is initialized with a state estimate corresponding to a true state and an appropriate covariance matrix.

The proposed configuration of the EKF is used for estimation of the orientation of a single segment on which an IMU is attached. For a valid estimation the linear acceleration of the joint connecting the previous segment must be known. With a recursive procedure processing segment by segment the orientation of any number of segments in kinematic chain can be determined. For the initial segment in the chain either the orientation or the acceleration of mounting point need to be known. It is convenient to constrain the motion such that the linear acceleration of the mounting point (joint) of the first segment is zero:

$${}^{S}\boldsymbol{a}_{1,1} = [0, 0, 0]^{T}. \tag{27}$$

For the following segments, the acceleration ${}^{S}\boldsymbol{a}_{1,j}$, which presents the input to the segment's EKF, is calculated by (8)–(11).

2.4. *Implementation of model-based EKF for human motion kinematics assessment*

For assessing the kinematic parameters in human walking a seven segment model of human body was utilized incorporating left and right foot, shank, thigh, and head–arm–trunk (HAT) segment. During walking each foot alternates between swing and stance phase. In stance phase, the foot which is in contact with the floor, is ensuring standstill condition (27) for the initial joint point. The leg, which is in contact with the floor, is thus considered to be the first segment in the kinematic chain. During walking, with alternating the swing and the stance phases also the first segment in the chain is alternating between the left and the right foot.

Table 1 – Subjects' demographic data and size of the insoles.

Subject	Sex	Age [years]	Height [m]	Weight [kg]	Insole size [EU]
S1	M	30	1.78	74	43/44
S2	M	24	1.70	74	39/40
S3	M	27	1.86	90	43/44
S4	M	32	1.75	70	39/40
S5	M	25	1.87	82	43/44

Please cite this article in press as: S. Šlajpah, et al., Kinematics based sensory fusion for wearable motion assessment in human walking, Comput. Methods Programs Biomed. (2013), http://dx.doi.org/10.1016/j.cmpb.2013.11.012

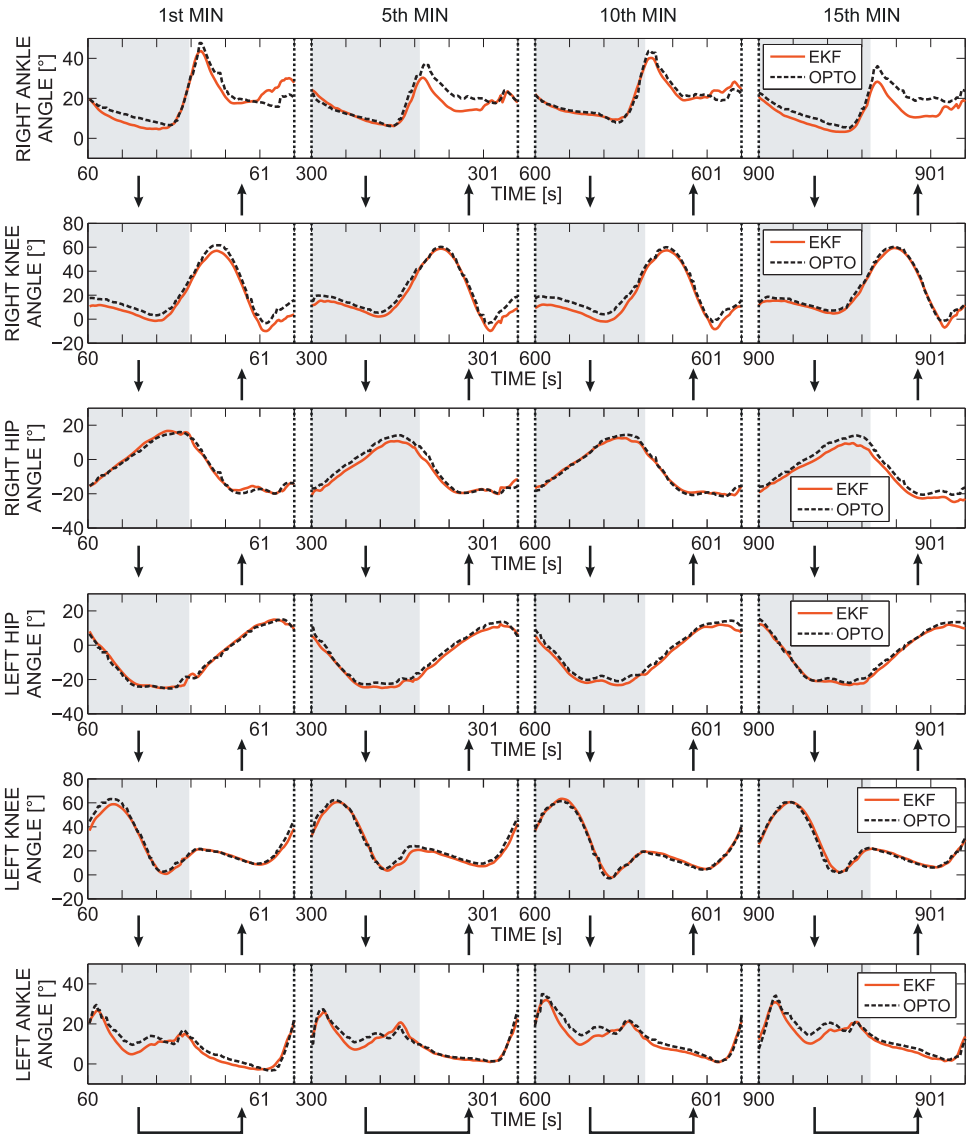

Fig. 4 – Right and left ankle, knee, and hip joint angle trajectories during one step determined by proposed model-based EKF algorithm (solid line) and reference Optotrak system (dashed line) in 1st, 5th, 10th, and 15th minute at walking speed 4 km/h. Grey areas denote RL direction of calculation while white areas denote LR direction. Change of calculation direction occurs at instant of transition of the rear leg from stance into swing phase.

Table 2 – Pearson's correlation coefficient between assessed and reference joint angles for ankle r_{AN}, knee r_{KN}, and hip r_{HP} at different speeds of walking on a treadmill and walking on a polygon with stairs. Coefficients are presented as mean (standard deviation).

Walking speed	r_{AN}	r_{KN}	r_{HP}
Right side			
4 km/h	0.89 (0.04)	0.94 (0.02)	0.97 (0.01)
6 km/h	0.77 (0.06)	0.92 (0.01)	0.96 (0.02)
Polygon	0.84 (0.08)	0.97 (0.02)	0.99 (0.01)
Left side			
4 km/h	0.86 (0.05)	0.92 (0.02)	0.97 (0.01)
6 km/h	0.71 (0.04)	0.89 (0.01)	0.96 (0.01)
Polygon	0.82 (0.07)	0.97 (0.02)	0.96 (0.03)

A recursive algorithm composed of seven EKFs is implemented for the estimation of the individual segments orientation. Local coordinate frames of each individual segment on a seven segment model are noted in Fig. 2a. When the right foot is in the stance phase the recursive algorithm incorporating seven EKFs is calculated in the right–left (RL) direction as illustrated in Fig. 2b: (1) right foot, (2) right shank, (3) right thigh, (4) HAT, (5) left thigh, (6) left shank, and (7) left foot. In the situation when the left foot is in the stance phase, the direction of the recursive calculation is reversed and goes from the left foot up to the right foot (LR direction, see Fig. 2c). With reversed direction of calculation also the vectors describing IMUs placement on the segment are reversed.

The instant of switching between calculation directions is determined as the instant of transition of the rear leg from stance into swing phase. Since at that moment the front leg is

Please cite this article in press as: S. Šlajpah, et al., Kinematics based sensory fusion for wearable motion assessment in human walking, Comput. Methods Programs Biomed. (2013), http://dx.doi.org/10.1016/j.cmpb.2013.11.012

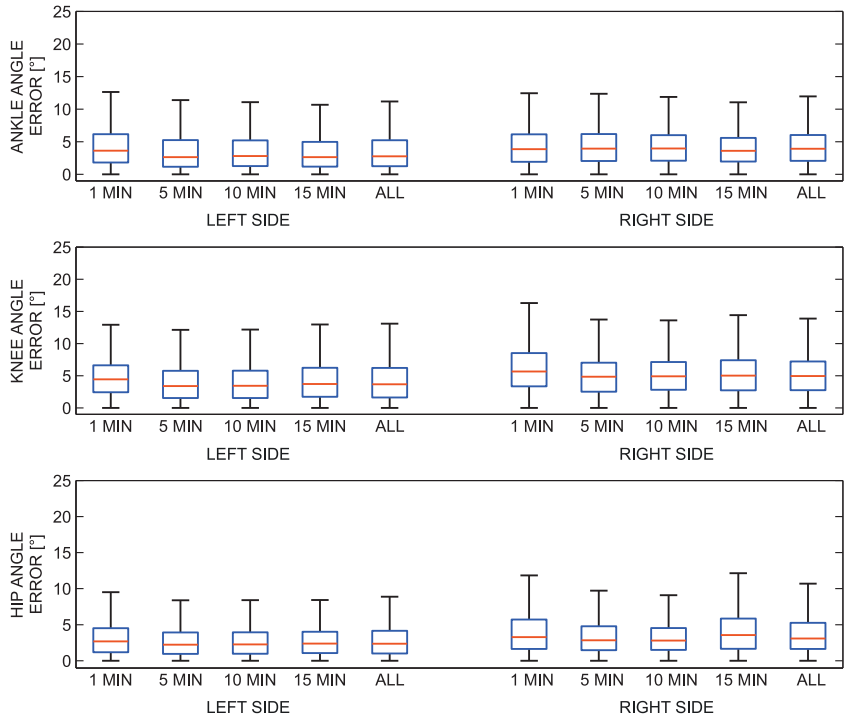

Fig. 5 – Absolute error between assessed and reference joint angle trajectories for ankles, knees, and hips during 1st (1 MIN), 5th (5 MIN), 10th (10 MIN), 15th (15 MIN) minute and during whole trail (ALL) for all trails accomplished at walking speed 4 km/h. The middle line, the bottom and the top of the box present median, 25th and 75th percentile, respectively. The whiskers present the furthermost value in the 1.5 interquartile ranges.

already in contact with the floor, the high impact deceleration of the heel strike is disregarded in the first segment orientation estimation. While the first segment is in a stance phase, the center point of the foot contact, which is considered as an origin with zero acceleration, is moving from the heel towards the toes. The position of the contact center point (foot center of pressure – COP) is measured by instrumented shoe insoles. By knowing the position of the COP and the height of the IMU placement on the foot ${}^{S}h_j$, the vector pointing from the sole to the IMU is constructed as

$$ {}^{S}\boldsymbol{r}_{1,1} = [{}^{S}\mathrm{COP}_{X,1}, {}^{S}h_1, {}^{S}\mathrm{COP}_{Z,1}]^{T} \quad (28) $$

where ${}^{S}\mathrm{COP}_{X,j}$ and ${}^{S}\mathrm{COP}_{Z,j}$ denote COP X and Y coordinates with respect to foot coordinate system (see Fig. 2a). Similar to (28) the vector ${}^{S}\boldsymbol{r}_{2,7}$ is determined.

3. Experimental validation and results

3.1. *Experimental protocol*

An experimental evaluation of long-term human walking was accomplished in order to test the accuracy and long-term reliability of developed model-based EKF algorithm. Long-term walking was measured at treadmill at two different speeds of 4 and 6 km/h to validate the algorithm performance under different dynamic conditions. Besides, the algorithm was tested during long-term walking on a round polygon with stairs simulating different types of everyday walking activities. The polygon was set as a round path composed of a 10 m of flat walking surface followed by 3 stairs, a 1.5 m of elevated walking path and additional 3 stairs, total 13 m in length (see Fig. 3c). The evaluation thus involved level walking, stair climbing, turning and stair ascending. For the reference, optical measurement system Optotrak (Northern Digital Inc., Waterloo, Canada) was used measuring the absolute positions of active infrared markers attached at the anatomical landmarks of human body and IMUs. In walking on the polygon only two steps before the stairs and steps on stairs were captured with the reference system due to limited measuring area of the Optotrak.

Five males (27.6 ± 3.4 years old, 1.79 ± 0.07 m height, 78 ± 8 kg weight (mean ± standard deviation)) were representing a test group. Their demographic data and sizes of used insoles are collected in Table 1. None of participants had any known history of severe lower-limb trauma or neurological disease. All subjects signed an informed consent before participating in the study. The experiment was accomplished in the framework of a research program approved by the Slovenian medical ethics committee.

IMUs were mounted on a plastic plate together with three infrared reference markers as shown in Fig. 3b. Measuring plates were firmly fixed on the segments of lower extremities (feet, shanks, thighs) and lower back by velcro straps in a way that coordinate axes of the IMU were approximately aligned with axes of the segmental frame (see Fig. 3a). Rotational matrices between IMUs and segments ${}^{S}\mathbf{R}_I$ were identified and

Please cite this article in press as: S. Šlajpah, et al., Kinematics based sensory fusion for wearable motion assessment in human walking, Comput. Methods Programs Biomed. (2013), http://dx.doi.org/10.1016/j.cmpb.2013.11.012

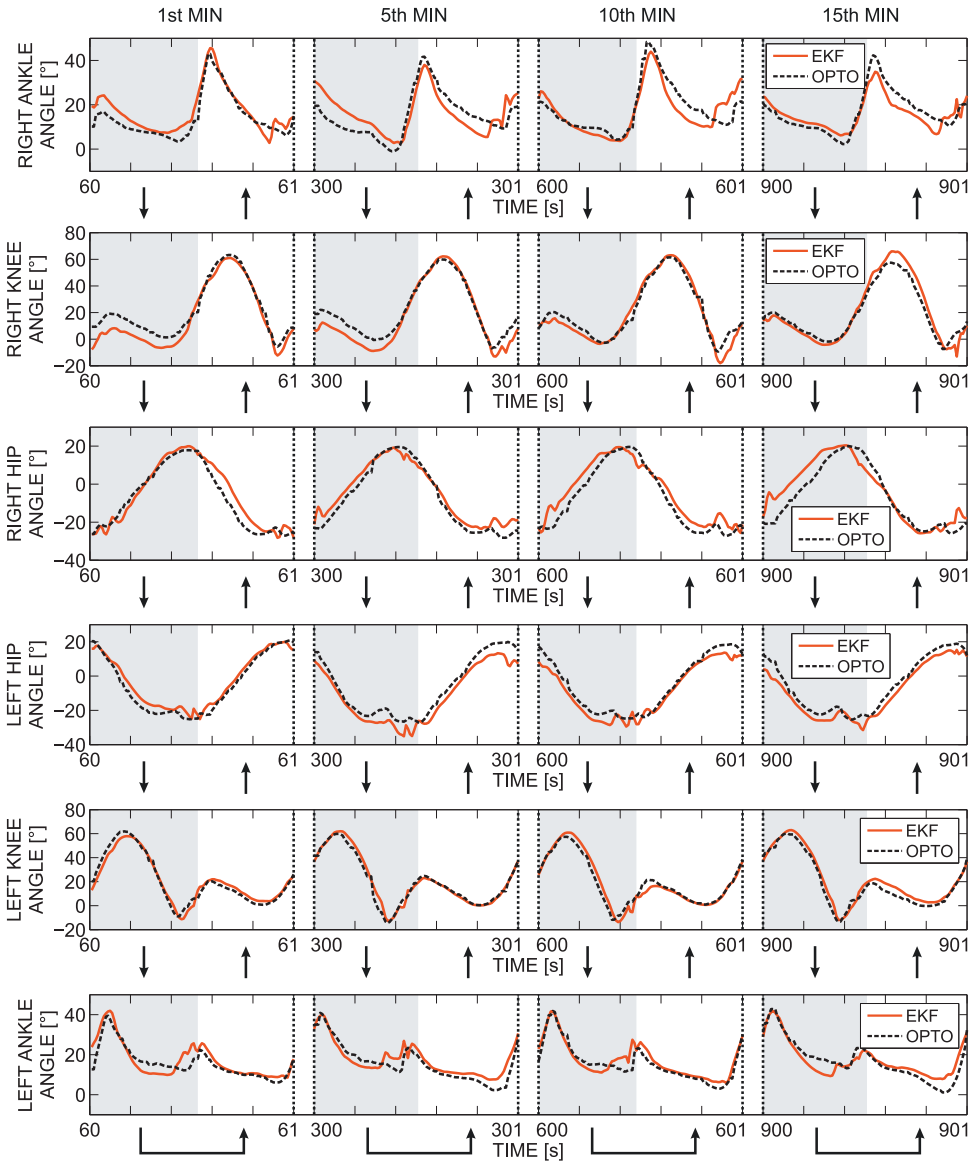

Fig. 6 – Right and left ankle, knee, and hip joint angle trajectories during one step determined by proposed model-based EKF algorithm (solid line) and reference Optotrak system (dashed line) in 1st, 5th, 10th, and 15th minute at walking speed 6 km/h. Grey areas denote RL direction of calculation while white areas denote LR direction. Change of calculation direction occurs at instant of transition of the rear leg from stance into swing phase.

transformed into quaternions ${}^{S}\boldsymbol{q}_{I}$ for use in Eqs. (3)–(5). In addition, reference infrared measuring markers were placed over the anatomical landmarks describing centers of ankle, knee and hip joints. Subjects were fitted with the proper size of the Parotec-System insoles.

In the first set of test trials subjects were asked to walk on a treadmill two times for 15 min; each time at a different speed. A normal walking speed was considered to be 4 km/h, while fast walking was accomplished at speed of 6 km/h. In the second set subjects walked on the polygon at self selected speed. Raw signals from IMUs, insoles and Optotrak were all sampled synchronically with sample rate of 100 Hz.

Vectors ${}^{S}\boldsymbol{r}_{1,j}$ and ${}^{S}\boldsymbol{r}_{2,j}$ describing IMUs placement on the segments were obtained on a basis of information from reference measurement system. Estimates of the segments' orientations, presented with quaternions ${}^{E}\boldsymbol{q}_{j}$, were calculated by the developed model-based EKF. Reference orientations of the segments were calculated from information about three markers placed on the measuring plates.

Reference and estimated joint angles were determined as the rotational differences between measured orientations of two neighboring segments: ankle angle as difference between foot and shank orientation, knee angle as difference between shank and thigh orientations, and hip angle as difference between thigh and HAT orientations.

Absolute error between estimated and reference joint angles at different time frames (in 1st, 5th, 10th, and 15th minute) were used to assess the algorithm accuracy and long-term reliability. In addition, similarity between estimated and reference joint angle trajectories during whole trail were

Please cite this article in press as: S. Šlajpah, et al., Kinematics based sensory fusion for wearable motion assessment in human walking, Comput. Methods Programs Biomed. (2013), http://dx.doi.org/10.1016/j.cmpb.2013.11.012

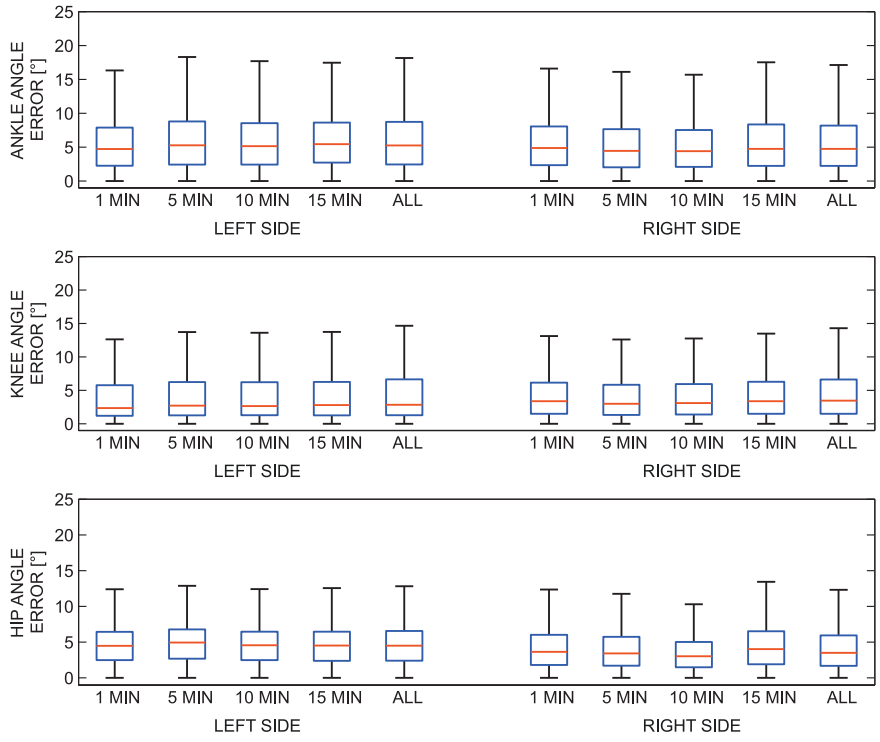

Fig. 7 – Absolute error between assessed and reference joint angle trajectories for ankles, knees, and hips during 1st (1 MIN), 5th (5 MIN), 10th (10 MIN), 15th (15 MIN) minute and during whole trail (ALL) for all trails accomplished at walking speed 6 km/h. The middle line, the bottom and the top of the box present median, 25th and 75th percentile, respectively. The whiskers present the furthermost value in the 1.5 interquartile ranges.

statistically assessed with calculation of Pearson's correlation coefficient r. Value of the r lies in a range $r \in [-1, 1]$, where 1 represents identical shapes of two compared signals. All data processing was accomplished using Matlab R2013a software (MathWorks, USA).

3.2. Results

Kinematic analysis of long-term gait encompassed comparison of joint angles of lower extremities assessed by proposed EKF algorithm and reference Optotrak system. In the results, joint angles with largest range of motion were analysed: dorsiflexion/plantar flexion of the ankle, extension/flexion of the knee and extension/flexion of the hip. To test the reliability of the proposed algorithm the error was evaluated in 1st, 5th, 10th and 15th minute of the walking on the treadmill trail and on the polygon with stairs.

Results are illustrated with two kinds of graphs. First, typical joint angle trajectories for the right and left ankle, knee, and hip assessed by the proposed algorithm and reference system are presented in four time slots (1st, 5th, 10th, and 15th minute of the experiment). RL and LR directions of calculations are marked with grey and white areas, respectively. The recursive procedure and calculation direction are denoted with arrows. Second, long-term reliability is evaluated as a statistical representation of absolute errors between assessed and reference joint angles at different time steps (at minute 1, 5, 10, and 15) in a duration of 1 min. The absolute joint angle errors are presented with boxplots for the 1st, 5th, 10th, 15th minute and over the whole trail (denoted as 1 MIN, 5 MIN, 10 MIN, 15 MIN, and ALL, respectively). Boxplots are presented separately for the left and the right ankle, knee and hip joint angles.

Comparison of typical joint angle trajectories for normal speed of walking (4 km/h) for the subject S4 is illustrated in Fig. 4. Each time slot covers one step (double stance – left leg swing – double stance – right leg swing – double stance) with duration of 1.2 s. In Fig. 5 the absolute joint angle errors of all trails ($n = 5, 744 \pm 57$ steps per trail, 1.24 ± 0.10 s duration of one step) of 4 km/h are presented with boxplots.

Comparison of typical joint angle trajectories for walking at speed of 6 km/h which is considered dynamic walking is illustrated in Fig. 6. Trajectories show one step in duration of 1 s at four time slots. Statistical representation of absolute errors between assessed and reference joint angles for all trails ($n = 5, 906 \pm 36$ steps per trail, 1.01 ± 0.04 s duration of one step) accomplished at walking speed 6 km/h is shown in Fig. 7.

In testing on a polygon with stairs on average 647 ± 114 m of distance was covered with the speed of 2.6 ± 0.5 km/h. Comparison of typical joint angle trajectories for knees, ankles, and hips for the subject S1 is illustrated in Fig. 8. Trajectories show half of the preparation step and climbing of 3 stairs in duration of approximately 3 s. In addition, feet contact durations are marked on the graphs for the left and right side by thick solid lines. Absolute errors between assessed and reference joint angles for all trails ($n = 5, 49.8 \pm 8.8$ rounds per trail, 18.6 ± 3.9 s duration of one round) are shown in Fig. 9.

Please cite this article in press as: S. Šlajpah, et al., Kinematics based sensory fusion for wearable motion assessment in human walking, Comput. Methods Programs Biomed. (2013), http://dx.doi.org/10.1016/j.cmpb.2013.11.012

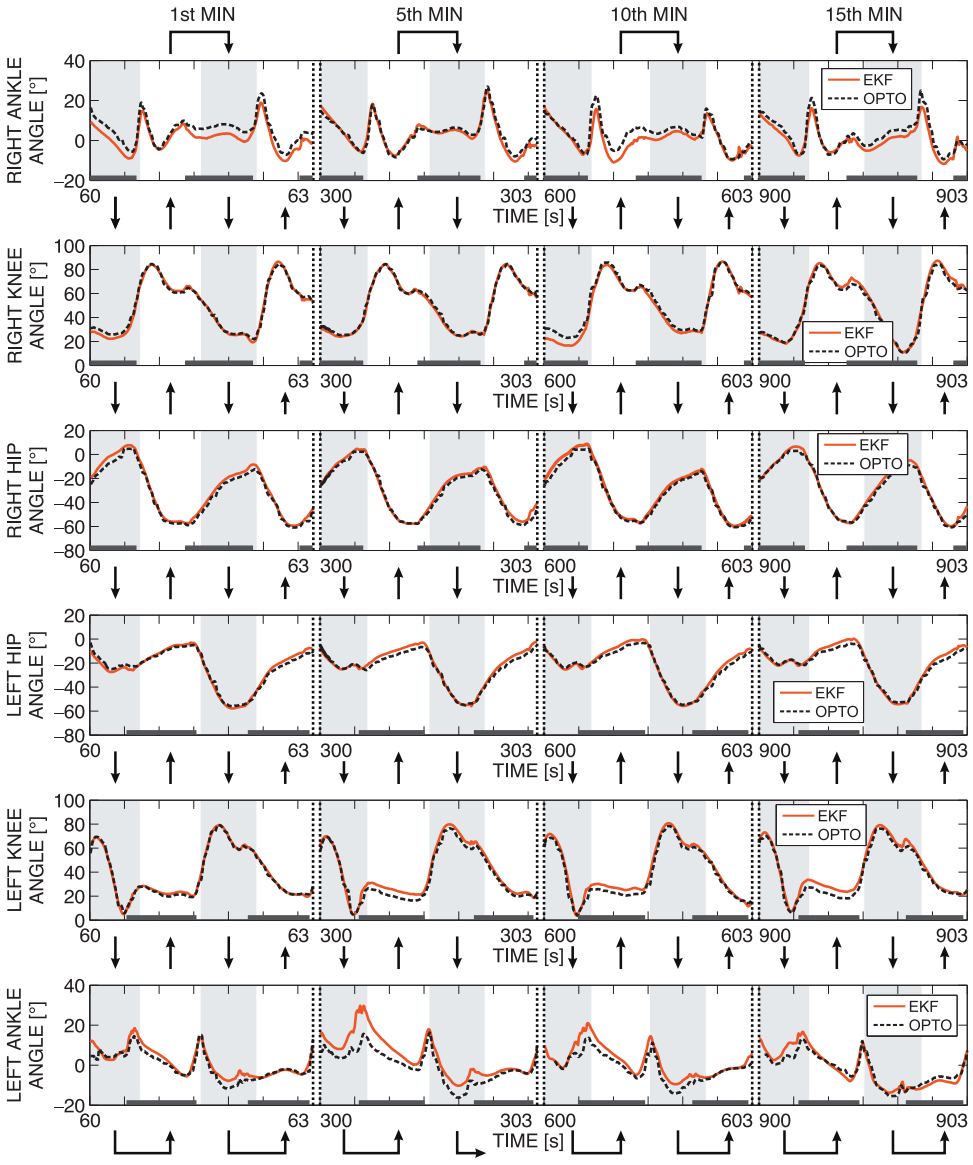

Fig. 8 – Right and left ankle, knee, and hip joint angle trajectories during half of the preparation step and stair climbing determined by proposed model-based EKF algorithm (solid line) and reference Optotrak system (dashed line) in 1st, 5th, 10th, and 15th minute of walking on polygon with stairs. Grey areas denote RL direction of calculation while white areas denote LR direction. Thick solid lines represent feet contact durations for each time frame as followed: right foot: floor–1st stair–3rd stair; left foot: floor–2nd stair.

Table 2 shows mean Pearson's correlation coefficients with standard deviation which are describing the similarity of assessed and reference joint angle trajectories for the left and the right ankles, knees, and hips. Comparison is presented separately for walking on a treadmill with walking speeds 4 and 6 km/h and walking on a polygon with stairs.

4. Discussion

A wearable sensory system and algorithm for kinematic parameters assessment in long-term and dynamic human walking is presented in this paper. Sensory system utilizes inertial and magnetic measurement units and force measurement insoles. A model-based extended Kalman filter is introduced which is based upon the kinematic relation between linear acceleration and angular velocity of a rigid body. The novelty is that in this way a constant fusion of measured inertial signals is enabled. The presented concept use accelerometer data for continuous fusion, and not just for inclination estimation during quasi-static conditions as presented in many other papers [17–19,24–29,32]. With a novel EKF, a recursive algorithm is proposed treating the lower extremities of a human as a serial kinematic chain which opens alternatingly with a swinging leg. Due to EKF requirement for known linear acceleration of the contact point of the first segment, a switching algorithm based on foot loading information was introduced.

Please cite this article in press as: S. Šlajpah, et al., Kinematics based sensory fusion for wearable motion assessment in human walking, Comput. Methods Programs Biomed. (2013), http://dx.doi.org/10.1016/j.cmpb.2013.11.012

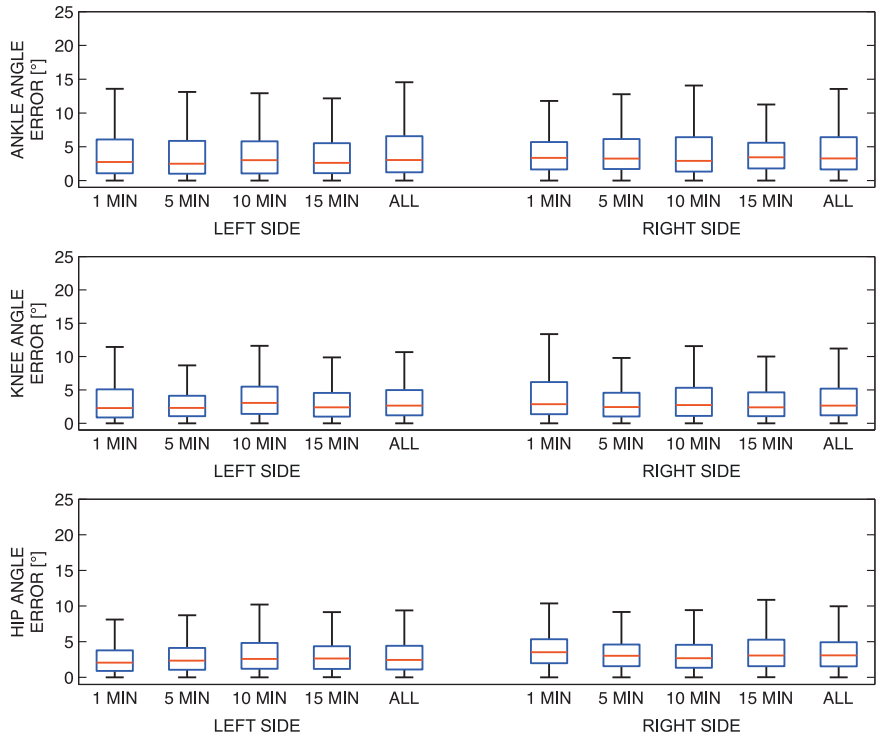

Fig. 9 – Absolute error between assessed and reference joint angle trajectories for ankles, knees, and hips during 1st (1 MIN), 5th (5 MIN), 10th (10 MIN), 15th (15 MIN) minute and during whole trail (ALL) for all trails accomplished at walking on the polygon with stairs. The middle line, the bottom and the top of the box present median, 25th and 75th percentile, respectively. The whiskers present the furthermost value in the 1.5 interquartile ranges.

For validation of algorithm performance, a series of long-term walking trials were performed on a treadmill at two different speeds and on a polygon with stairs. Assessed ankle, knee, and hip joint angle trajectories were compared to the reference values acquired with the reference optical system. The comparison of joint angle trajectories acquired at normal walking speed 4 km/h shows that model-based EKF algorithm is capable to track the knee and hip joint angle trajectories consistently throughout long-term walking. Also, the medians of the overall absolute angle error are low with values about 3.7°, 3.9°, 2.3°, and 3.0° for the left and the right knee and hip joint angles, respectively (see Fig. 5). The results demonstrate performance comparable with other algorithms for joint angle assessment [19,18,31,27]. Concerning the ankle angle assessment, larger deviations from reference can be observed. Larger deviations are attributed to higher hell strike accelerations. However, the resulting orientation errors are still in the range of accepting values. Results of long-term reliability evaluation show that the median of the absolute angle error stays stable throughout whole measurement trial with no expressed tendency of increasing with time. This is additionally confirmed with high calculated correlation coefficients (mean value for knee and hip joint angles is >0.92).

Long-term walking on a treadmill with the walking speed 6 km/h was performed to test the algorithm performance in dynamic conditions. The results show that larger deviations between wearable and reference outputs are present. Although the median of the absolute angle error is similar to the one achieved in normal walking, the larger scatter of errors can be observed (see Fig. 7). The reason for higher assessed joint angle deviations from reference values can be attributed to a shorter step with a faster swing phase of the leg and higher accelerations at heel strikes. Because the series of EKFs is interrelated, the error of the estimated orientation of the foot is effecting the following orientation estimates. The long-term reliability of the proposed approach evaluated in dynamic walking conditions is proved in Fig. 7. From figure it is evident that median values of absolute angle errors are not expressing tendency to increase with time. Correlation coefficients confirm high similarity between assessed and reference trajectories even in dynamic walking.

Long-term walking on the polygon simulated different everyday motion types: level walking, stair negotiation, and turning. The experiment tested the performance of the presented algorithm when combining different motion types and evaluated the long-term reliability. The comparison of joint angles trajectories shows that the performance of the proposed algorithm is not affected by changing the type of motion. The median errors of 3.0°, 2.7°, 2.4°, 3.3°, 2.6°, and 3.1° for the left and the right ankle, knee, and hip joint angles, respectively, validate the adequacy of the model-based EKF algorithm for tracking kinematic parameters in different motion conditions. From results, no tendency for increasing of median error can be observed. The close fit of the joint angles trajectories assessed with the wearable and with the reference system is additionally confirmed with the high correlation coefficients with mean of 0.93.

Please cite this article in press as: S. Šlajpah, et al., Kinematics based sensory fusion for wearable motion assessment in human walking, Comput. Methods Programs Biomed. (2013), http://dx.doi.org/10.1016/j.cmpb.2013.11.012

5. Conclusions

The presented paper introduces the novel sensory system and algorithms for kinematic parameters assessment of long-term human walking by model-based extended Kalman filter. The results of the experimental validation demonstrate that the proposed algorithm is capable to assess joint angles in human walking and other daily activities with the accuracy below 5° and consistently without tendency of error increasing with time. As demonstrated, the wearable system is appropriate for measuring kinematic parameters in long-term, uninterupted human motion od different dynamics. We have shown that kinematic parameters in regular daily activities such as level walking, stair negotiation, and turning can also be accessed by our approach. The only condition to be met for proper operation is that at least one foot must be in contact with the floor at any given time. During regular walking, this condition is inherently met qualifying our approach as appropriate. For motions which include a ballistic phase (e.g. running) the performance of our algorithm would significantly decrease. The proposed model-based EKF algorithm is suitable for walking analyzes and also for providing essential feedback within the control system of wearable robots. The proposed novel approach is also applicable in other areas of mechatronics where orientation assessment of serially linked segments is of interest.

Conflict of interest

There are no conflicts of interest.

Acknowledgements

This study was supported by the Slovenian Research Agency (ARRS) under Grant 1000-11-310147 and research programme Motion analysis and synthesis in man and machine (P2-0228), and partially by the EU project CYBERLEGs FP7-ICT-2011-7-287894.

REFERENCES

[1] P. Bonato, Wearable sensors/systems and their impact on biomedical engineering, IEEE Engineering in Medicine and Biology Magazine 22 (3) (2003) 18–20.
[2] E.C. Martinez-Villalpando, H. Herr, Agonist-antagonist active knee prosthesis: a preliminary study in level-ground walking, Journal of Rehabilitation Research & Development 46 (3) (2009) 361–373.
[3] F. Sup, A. Bohara, M. Goldfarb, Design and control of a powered transfemoral prosthesis, International Journal of Robotics Research 27 (2) (2008) 263–273.
[4] J.C. Moreno, E.R. de Lima, A.F. Ruí z, F.J. Brunetti, J.L. Pons, Design and implementation of an inertial measurement unit for control of artificial limbs: application on leg orthoses, Sensors and Actuators B: Chemical 118 (1) (2006) 333–337.
[5] J.A. Blaya, H. Herr, Adaptive control of a variable-impedance ankle-foot orthosis to assist drop-foot gait, IEEE Transactions on Neural Systems and Rehabilitation Engineering 12 (1) (2004) 24–31.
[6] H. Kawamoto, S. Kanbe, Y. Sankai, Power assist method for HAL-3 estimating operator's intention based on motion information, in: Robot and Human Interactive Communication, 2003. Proceedings of ROMAN, 2003. The 12th IEEE International Workshop on, IEEE, 2003, pp. 67–72.
[7] H. Kazerooni, The Berkeley lower extremity exoskeleton, in: Field and Service Robotics, Springer, Berlin, Heidelberg, 2006, pp. 9–15.
[8] P.N. Page, D. Hawkins, A real-time biomechanical feedback system for training rowers, Sports Engineering 6 (2) (2003) 67–79.
[9] L. Chiari, M. Dozza, A. Cappello, F.B. Horak, V. Macellari, D. Giansanti, Audio-biofeedback for balance improvement: an accelerometry-based system, IEEE Transactions on Biomedical Engineering 52 (12) (2005) 2108–2111.
[10] S. Crea, N. Vitiello, S.M.M. De Rossi, T. Lenzi, M. Donati, C. Cipriani, M.C. Carrozza, Development of an experimental set-up for providing lower-limb amputees with an augmenting feedback, in: Converging Clinical and Engineering Research on Neurorehabilitation, Springer, Berlin, Heidelberg, 2013, pp. 321–325.
[11] R. Kamnik, T. Bajd, Standing-up robot: an assistive rehabilitative device for training and assessment, Journal of Medical Engineering & Technology 28 (2) (2004) 74–80.
[12] E. Van Asseldonk, R. Ekkelenkamp, J. Veneman, F. Van der Helm, H. Van der Kooij, Selective control of a subtask of walking in a robotic gait trainer (LOPES), in: Rehabilitation Robotics, 2007. ICORR 2007. IEEE 10th International Conference on, IEEE, 2007, pp. 841–848.
[13] A. Tsukahara, Y. Hasegawa, Y. Sankai, Standing-up motion support for paraplegic patient with robot suit HAL, in: Rehabilitation Robotics, 2009. ICORR 2009. IEEE International Conference on, IEEE, 2009, pp. 211–217.
[14] D.A. Winter, Biomechanics and Motor Control of Human Gait: Normal, Elderly and Pathological, University of Waterloo Press, Waterloo, 1991.
[15] M.W. Whittle, Gait Analysis: An Introduction, Butterworth-Heinemann, Oxford, 1996.
[16] K. Tong, M.H. Granat, A practical gait analysis system using gyroscopes, Medical Engineering & Physics 21 (2) (1999) 87–94.
[17] R. Williamson, B. Andrews, Detecting absolute human knee angle and angular velocity using accelerometers and rate gyroscopes, Medical and Biological Engineering and Computing 39 (3) (2001) 294–302.
[18] T. Liu, Y. Inoue, K. Shibata, Development of a wearable sensor system for quantitative gait analysis, Measurement 42 (7) (2009) 978–988.
[19] R.E. Mayagoitia, A.V. Nene, P.H. Veltink, Accelerometer and rate gyroscope measurement of kinematics: an inexpensive alternative to optical motion analysis systems, Journal of Biomechanics 35 (4) (2002) 537–542.
[20] A.T.M. Willemsen, J. Van Alste, H. Boom, Real-time gait assessment utilizing a new way of accelerometry, Journal of Biomechanics 23 (8) (1990) 859–863.
[21] H. Dejnabadi, B.M. Jolles, K. Aminian, A new approach to accurate measurement of uniaxial joint angles based on a combination of accelerometers and gyroscopes, IEEE Transactions on Biomedical Engineering 52 (8) (2005) 1478–1484.
[22] M.D. Djurić-Jovičić, N.S. Jovičić, D.B. Popović, Kinematics of gait: new method for angle estimation based on accelerometers, Sensors 11 (11) (2011) 10571–10585.
[23] K. Liu, T. Liu, K. Shibata, Y. Inoue, R. Zheng, Novel approach to ambulatory assessment of human segmental orientation on a wearable sensor system, Journal of Biomechanics 42 (16) (2009) 2747–2752.
[24] H. Luinge, P.H. Veltink, Measuring orientation of human body segments using miniature gyroscopes and

accelerometers, Medical and Biological Engineering and Computing 43 (2) (2005) 273–282.
[25] H. Dejnabadi, B.M. Jolles, E. Casanova, P. Fua, K. Aminian, Estimation and visualization of sagittal kinematics of lower limbs orientation using body-fixed sensors, IEEE Transactions on Biomedical Engineering 53 (7) (2006) 1385–1393.
[26] J. Favre, B. Jolles, O. Siegrist, K. Aminian, Quaternion-based fusion of gyroscopes and accelerometers to improve 3d angle measurement, Electronics Letters 42 (11) (2006) 612–614.
[27] R. Takeda, S. Tadano, A. Natorigawa, M. Todoh, S. Yoshinari, Gait posture estimation using wearable acceleration and gyro sensors, Journal of Biomechanics 42 (15) (2009) 2486–2494.
[28] P. Veltink, P. Slycke, J. Hemssems, R. Buschman, G. Bultstra, H. Hermens, Three dimensional inertial sensing of foot movements for automatic tuning of a two-channel implantable drop-foot stimulator, Medical Engineering & Physics 25 (1) (2003) 21–28.
[29] K.J. O'Donovan, R. Kamnik, D.T. O'Keeffe, G.M. Lyons, An inertial and magnetic sensor based technique for joint angle measurement, Journal of Biomechanics 40 (12) (2007) 2604–2611.
[30] D. Roetenberg, H.J. Luinge, C.T. Baten, P.H. Veltink, Compensation of magnetic disturbances improves inertial and magnetic sensing of human body segment orientation, IEEE Transactions on Neural Systems and Rehabilitation Engineering 13 (3) (2005) 395–405.
[31] D. Roetenberg, P.J. Slycke, P.H. Veltink, Ambulatory position and orientation tracking fusing magnetic and inertial sensing, IEEE Transactions on Biomedical Engineering 54 (5) (2007) 883–890.
[32] T. Beravs, P. Rebersek, D. Novak, J. Podobnik, M. Munih, Development and validation of a wearable inertial measurement system for use with lower limb exoskeletons, in: Humanoid Robots (Humanoids), 2011 11th IEEE-RAS International Conference on, IEEE, 2011, pp. 212–217.
[33] D. Roetenberg, H. Luinge, P. Slycke, Xsens MVN: full 6DOF human motion tracking using miniature inertial sensors, Xsens Motion Technologies BV, Tech. Rep., 2009.
[34] K.J. Chesnin, L. Selby-Silverstein, M.P. Besser, Comparison of an in-shoe pressure measurement device to a force plate: concurrent validity of center of pressure measurements, Gait & Posture 12 (2) (2000) 128–133.
[35] R.E. Kalman, A new approach to linear filtering and prediction problems, Journal of Basic Engineering 82 (1) (1960) 35–45.
[36] W. Greg, B. Gary, An Introduction to the Kalman Filter, Department of Computer Science, University of North Carolina at Chapel Hill, North Carolina, 2006.
[37] A.J. Hanson, Visualizing quaternions, in: ACM SIGGRAPH 2005 Courses, ACM, 2005.

Please cite this article in press as: S. Šlajpah, et al., Kinematics based sensory fusion for wearable motion assessment in human walking, Comput. Methods Programs Biomed. (2013), http://dx.doi.org/10.1016/j.cmpb.2013.11.012